Journal of Photochemistry & Photobiology, B: Biology 153 (2015) 51–58

Contents lists available at ScienceDirect

Journal of Photochemistry & Photobiology, B: Biology

journal homepage: www.elsevier.com/locate/jpb

Confocal Raman spectroscopy: *In vivo* biochemical changes in the human skin by topical formulations under UV radiation

M.G. Tosato [a], D.E. Orallo [b], S.M. Ali [c], M.S. Churio [b], A.A. Martin [c], L. Dicelio [a,*]

[a] Institute of Physical Chemistry of Materials, Environment and Energy, Faculty of Exact and Natural Sciences, University of Buenos Aires, Ciudad Universitaria s/n Pabellón II, C1428EHA Capital Federal, Argentina
[b] Department Chemistry, Faculty of Exact and Natural Sciences, National University of Mar del Plata, Dean Funes 3350, B7602AYL Mar del Plata, Argentina
[c] Laboratory of Biomedical Vibrational Spectroscopy, Universidade do Vale do Paraíba — UNIVAP, Shishima Hifumi 2911, 12244000 Sao José dos Campos, Brazil

ARTICLE INFO

Article history:
Received 18 May 2015
Received in revised form 12 August 2015
Accepted 30 August 2015
Available online 1 September 2015

Keywords:
Confocal Raman
Human skin
Mycosporine-like amino acids
Gadusol
Urocanic acid
UV radiation

ABSTRACT

A new approach to the study of the effects on human skin of mycosporine-like amino acids (MAAs) and gadusol (Gad) incorporated in polymer gel is proposed in this work. The depth profile and photoprotector effects of Pluronic F127® gels containing each of the natural actives were evaluated by *in vivo* confocal Raman spectroscopy aiming at the analysis of the biochemical changes on human skin. Hierarchical cluster analysis (HCA) showed that the data corresponding to different depths of the skin, from surface to 4 μm, and from 6 to 16 μm, remained in the same cluster. *In vivo* Raman spectra, classified into five different layers of epidermis according to their similarities, indicated that the amount of Gad gel increased by about 26% in the outermost layer of the stratum corneum (SC) and that MAAs gel at 2 μm depth was 103.4% higher than in the outermost layer of the SC. Variations in the SC of urocanic acid at 1490–1515 cm^{-1} and 1652 cm^{-1} and histidine at 1318 cm^{-1} were calculated, before and after UV exposure with or without gels. With the application of gels the vibrational modes that correspond to lipids in *trans* conformation (1063 and 1128 cm^{-1}) increased with respect to normal skin, whereas *gauche* conformation (1085 cm^{-1}) disappeared. Our studies suggest that gels protected the skin against the stress of the natural defense mechanism caused by high levels of UV exposure.

1. Introduction

The skin provides the principal barrier to the external environment. It is exposed to oxidative stress both from endogenous and exogenous sources such as ultraviolet radiation (UV), which promotes wrinkle formation and loss of tissue elasticity. Most UV rays, which penetrate into the human skin, are absorbed by the chromophores of epidermis, and only the longer wavelengths are transmitted through the dermis. Several chromophores, which absorb the UV or visible radiation, initiate the biological responses including DNA, urocanic acid, amino acids, melanins and their precursors, and metabolites [1]. To induce immune suppression, the electromagnetic energy of UV radiation must be absorbed by an epidermal photoreceptor and converted into a biological recognizable signal [2]. There is evidence that UVB radiation (280–315 nm) directly damages DNA yielding photoproducts such as those formed by adjacent thymine bases, whereas chronic exposure to UVA light (315–400 nm) can cause premature aging and cancer of the skin by inducing the production of reactive oxygen species (ROS) [3,4]. ROS include singlet oxygen ($^1O_2$), superoxide radical ($O_2^{\bullet -}$), hydrogen peroxide (H_2O_2), and hydroxyl radical ($OH^{\bullet -}$) species that promote lipid, protein, DNA, and RNA oxidation. All these processes are involved in most of the biological effects caused by UV exposure, such as photocarcinogenesis, photoimmunosuppression, photoaging (development of both deep wrinkles and a marked loss of elasticity), sunburn, and photoallergy [5–7]. Urocanic acid (UCA), a major absorber of UV radiation, is produced in the upper layers of mammalian epidermis by the deaminating action of histidase on histidine (HIS) and is a major absorber of UV radiation [8,9]. Epidermal UCA is found predominantly as the *trans*-isomer. This isomer transforms to *cis*-UCA following exposure to UV light until a photostationary state is reached when the concentration of *cis*-UCA is about 60–70% of total UCA [10–12]. The quantum yield of the *trans* to *cis* ($\Phi_{t \rightarrow c}$) photoreaction is low, which generates an inefficient process of protection [12].

Wulf et al. suggested that natural photoprotection involves thickening of SC by sunlight and increased pigmentation [13]. The regular use of sunscreens have been found to exhibit protective effects against the different ROS involved in photoaging and photocarcinogenesis [14,15].

Recent studies have focused on marine organisms as a source of natural bioactive molecules with therapeutic properties. Porphyra-334 and shinorine, two mycosporine-like amino acids (MAAs) isolated from marine red algae (genus *Porphyra*), and gadusol (Gad), obtained from marine fish roes, are structurally related metabolites with photoprotective and antioxidant activities [16–18]. The photoprotective role of this family of natural compounds is supported by their strong absorption and high photostability in the UVA and UVB regions of solar radiation spectrum [17,18]. Moreover, Gad has been found to efficiently deactivate

* Corresponding author.

http://dx.doi.org/10.1016/j.jphotobiol.2015.08.030
1011-1344/

photosensitizers and is comparable to ascorbic acid towards reductive reactions of radical species [16,17]. Thus, potential application of these marine compounds has been suggested for prevention and therapeutic treatment of diseases related to the production of free radicals and UV irradiation of the skin. In this context, recent studies have assessed the protective effect of MAAs on human skin fibroblast cells [19]. The authors found that porphyra-334 is able to prevent photoaging by suppressing ROS production and inhibiting the expression of proteases involved in the photoaging of the skin under UV-A exposure [20,21]. In addition, *in vivo* evaluation of the cutaneous photoprotective ability of the MAA porphyra-334 and shinorine was carried out in mouse skin by de la Coba et al. [7]. According to their results, the mixture of MAAs prevented sunburn cell formation and structural and morphological alterations observed in biopsies of non-photoprotected skin. However, to the best of our knowledge, *in vivo* determinations of the effect natural actives based on MAAs and Gad on human skin have not been fully explored yet.

In vivo and non-invasive techniques in dermatology analysis are currently investigated to minimize the use of biopsies. Techniques such as videodermatoscopy, confocal microscopy, laser scanning microscopy, fluorescence lifetime imaging, dynamic infrared imaging, and optical coherence tomography provide fundamental knowledge about the layers of epidermis and superficial dermis, visualization of morphologic structures, and the effects of skin products [22–26]. Although the results are obtained in real time many methods present low specificity, and/or they require pigmented structures for analysis. Furthermore, the techniques do not provide details about the structure conformation of molecular constituents.

Raman spectroscopy has been widely used in recent years, especially for *in vivo* analysis, because it can offer direct molecular information of a sample without labeling, with the advantage of high spatial resolution (below 1 μm), and it is not affected by the interference of water signals. The Raman effect is based on inelastic scattering of light and was reported for the first time in liquids in 1928 by the Indian physicist Sir C.V. Raman [27]. A Raman spectrum is generally displayed by the wave number shift from incident laser to scattered photons against the scattering intensity, thus giving a unique characteristic for a specific chemical structure, comparable to a molecular fingerprint. For human skin, this technique has been applied for cancer diagnosis [28], analysis of physiological component distribution in skin tissue, permeation of cosmetic actives, skin decomposition [29,30], drug depth profiling [31] and biomechanical characterization of the SC [32,33].

In this study, we applied *in vivo* confocal Raman spectroscopy to investigate the biochemical effects of polymer gels containing Pluronic F-127® as delivery systems of MAAs and Gad in human skin. This triblock copolymer is commonly used in technological applications related to cosmetic and pharmaceutical industries [34,35]. Its biocompatibility and low toxicity make it suitable as a carrier for medical and pharmaceutical drug delivery [36,37].

2. Materials and Methods

2.1. MAA and Gadusol Extraction

MAAs were obtained from the red alga *Porphyra leucosticta* collected from the coast of Mar del Plata (Buenos Aires, Argentina) and stored at −20 °C until extraction with 50% ethanol:water. The extract was concentrated and treated with methanol in a sequence of evaporation, suspension, and centrifugation steps. The solid residue was dissolved in water and eluted with 50% methanol:water from an activated charcoal column. The fractions with maximal absorbance at 334 nm were collected and eluted with water from an ion exchange resin (Dowex 50W-X8). Finally, the purified samples were concentrated in a rotary evaporator and analyzed by High Performance Liquid Chromatography (HPLC) with an ODS (C18) column and aqueous mobile phase with 0.02% v/v acetic acid. Two major peaks were observed, and their retention times contrasted with standard samples, thus confirming the presence of the MAA known as shinorine and porphyra-334 at a concentration ratio of 1:4 [38].

Mature female gonads from the marine fish Argentine sandperch (*Pseudopercis semifasciata*) were used as the source of Gad. The extraction was carried out according to the procedure reported by Arbeloa et al. [18]. Briefly, the roes devoid of pelt were homogenized in ethanol and kept overnight at low temperature. The suspension was centrifuged, and after several cycles of filtering and new extraction with ethanol:water mixtures, the filtrates were combined and reduced in a rotary evaporator under vacuum. After successive washing steps with ethanol, chloroform, and water lots, the aqueous phase was concentrated and treated by ion-exchange chromatography on a Dowex 50W-X (8–400, H+ form) resin. The fractions containing gadusol were recognized by the reversible shift of the absorbance maximum from 268 to 296 nm on going from acid to neutral pH [39]. The presence of Gad was confirmed by HPLC analysis and contrasted with standard samples [18].

2.2. Gel Preparation

Gels containing the actives were prepared by using the "cold method" described by Schmolka [40]. A weighed amount of Pluronic F127® was slowly added to cold Milli-Q water (4–5 °C) by gentle mixing in order to obtain 8% w/v Pluronic 127® solutions. The samples were then frozen and kept overnight at 4 °C to form a macroscopically homogeneous and transparent solution. The actives were incorporated into different vials containing the aqueous phase gel up to 0.01% w/v of MAA and 0.01% w/v of Gad, respectively. The solutions were manually agitated and kept in the refrigerator.

2.3. Subjects

A total of 5 healthy subjects (females), age 20–30, with skin type II according to Fitzpatrick scale, without history of dermatological disease, participated in this study. The study was approved by the local ethics committee (CEP number 217948) and all subjects gave written informed consent. They were instructed to stop any topical application of cosmetics in the test area at least 12 h prior to the start of the study, and to withhold any exposure of the test area to artificial or natural UV-light at least 3 days before beginning the study. Raman spectra were recorded directly from the skin of the volar forearms.

2.4. Treatment

Three sites of 0.5 cm^2 each were delimited in the forearm to perform the Raman measurements. One area was used as a control, and each of other two were treated with 10 $\mu L/cm^2$ of the respective gel (MAA or Gad) formulation. UV exposure started 60 min after application of gel formulations. This treatment was repeated for 3 consecutive days.

2.5. UV radiation

UV irradiation was performed by using a Xenon lamp (Osram 24 V). A liquid filter was interposed to reduce the intensity within the IR wavelengths. The subjects were exposed for 15 min to approximately 1.3 J/cm^2 of UVA and UVB radiation [5,41]. The power of the radiation source was measured with a FM-GS Field Master meter (Coherent, USA). The dose used in this study is much smaller than 1 MED UVA (Minimal Erythema Doses) measured at 40° N Lat. during a full day in the summer [5].

2.6. Raman Spectroscopy

In vivo confocal Raman measurements were performed before and after UV exposure without and with gel applications. Before each test,

the subjects stayed in a climatized room (23 ± 1 °C and 55 ± 5% relative humidity) for at least 30 min. Before starting the treatment, two test sites on the volar forearm of normal skin were measured by confocal Raman spectrometer, and marked as 0.5 cm^2 areas with an adhesive tape. The subjects' forearms were positioned on the silica window on a metal platform after being cleaned with cotton soaked in 1.0 mL of 97% ethyl alcohol. Skin evaluations were performed by using an *in vivo* 3510 Skin Composition Analyzer (River Diagnostics, Rotterdam, The Netherlands) confocal spectrometer with an inverted microscope. Raman scattering was detected using a Peltier cooled (−70 °C) CCD detector (charge-coupled device) camera (128 × 1024 pixels), excited with vertically polarized 785 nm laser. The spectrometer equipped with diffraction gratings (600 grooves/mm), and the slit allowed the spectral resolution to be 4 cm^{-1} in the finger-print region (800–1800 cm^{-1}). The laser light focused on the sample with an oil immersion objective (40× NA 1.3). The laser power at the sample was measured and set to 23 mW, which is non-destructive for biological material. The area of the laser spot on the samples was 1 μm diameter. A video image (uEye camera software) was used to locate the accurate position of the laser spot on the volunteer's skin. Spectral acquisition and pre-processing were performed using RiverICon software. In order to obtain spectra in depth, the microscope objective was mounted on a piezoelectric translation stage equipped with a linear movement sensor, providing a spatial resolution of 2 μm. The depth profile for all treatment and control sites of the skin was conducted by using the following parameters: from 0 to 10 μm with 2 μm steps and 10 s integration time; from 10 to 56 μm with 5 μm steps and 20 s integration time. Two spectra were collected per depth and per volunteer.

2.7. Quantitative Analysis of Components

Raman data were acquired by means of RiverIcon® software version 2.5.2 and analyzed with Skin Tools® software v 2.0 (River Diagnostics). Raman spectra were pre-processed by baseline correction using a polynomial function of third or fifth order and following a Savitsky–Golay smoothing window of 5 or 7 points. The relative concentrations of *trans* urocanic acid (*t*-UCA) and histidine (HIS) *vs.* depth were calculated from the Raman spectra within 800–1800 cm^{-1} by using Lorentzian or Gaussian curve fitting.

In order to determine the biochemical changes in the skin due to the use of the gels, the areas of some peaks related to lipid and protein vibrations were evaluated. The curve-fitting procedure was based on Gaussian and Lorentzian functions. This method was used over several spectral regions, and the appropriate number of bands for the curve-fitting procedure was determined from the second derivative of the spectra. The accuracy of the fit was given by the chi-square (χ^2) value. The lower the value of the chi square, the better it fits [42]. Considerable care was taken in these experiments to minimize intrinsic changes by obtaining duplicate spectra. Similarly, the curve-fitting method was employed to obtain *in vivo* depth profiles of the areas treated with gels.

Other statistics methods were employed and the data presented as average ± standard deviation. The significance of differences in the data was evaluated by ANOVA test followed by T-Student. $P < 0.05$ values were considered statistically significant. The data analysis routines are contained in MINITAB® software. This includes multivariate reconstruction algorithms, for example, Hierarchical cluster analysis (HCA) and principal components analysis (PCA). HCA was performed to classify the spectral data on the PCA of the 1140–1374 cm^{-1} range. Hierarchical cluster analysis (HCA) was performed by using Ward's method and a dendrogram plot of the hierarchical binary cluster tree was generated to classify the mean spectral data for each skin layer.

3. Results

The hierarchical binary cluster tree obtained from de HCA allowed the classification of the mean spectral data for each skin layer. The results are shown by lines connecting data points, as a dendrogram plot. The height of each line represents the distance between the two data points. The distance represents the correlation between spot clusters. Spectra are grouped in clusters according to a similarity scale (Fig. 1). The variability between individuals was minimized by choosing the same skin type, age, and climate, but this was not enough. Therefore, the dendrogram was constructed on the basis of averaged spectra for each layer. The result of the clusters was satisfactory. The data from surface, 2 and 4 μm remained in the same cluster. The same occurred for 6, 11, and 16 μm. In the last two branches, we found that layers 41 and 51 μm showed reversed positions. This inversion of layers could be attributed to the similarity of their compositions.

Fig. 2a displays average *in vivo* Raman spectra in the fingerprint region of the SC and epidermis, which shows the clear biochemical differences between the skin layers. This region exhibits spectral features assigned to both lipids and proteins. The spectra were classified into five different layers of epidermis according to their similarities: stratum corneum-SC (surface to 16 μm), stratum granulosum — SG — (26 μm), stratum spinosum — SS — (36 and 41 μm) and basal (51 and 56 μm). The SC was divided into two parts named: stratum corneum — SC (surface, 2 and 4 μm) and stratum corneum II — SC2 (6, 11, and 16 μm). Spectra measured at 46 μm were not considered because this depth region is an interface between different layers.

Some clearly marked vibrational bands can be distinguished in the spectra. The main spectral bands of the each epidermis layer were assigned. Their respective location is shown in Fig. 2a and their assignments are shown in Table 1. The assignment of the bands in the Raman spectra of human skin was also based on previous publications [43–46].

The five layers display different spectral features. Several vibrational modes are observed that allow the molecular organization of human skin to be characterized. The uppermost layer is identified as the SC. The averaged spectrum of this layer shows the features of keratin with α-helix conformation (1655 cm^{-1}) and a lipid rich region (1063, 1128, 1297 and 1441 cm^{-1}) [43,44,47,48]. The weak peak at 1296 cm^{-1} arises from the CH_2 twisting mode of all-*trans* acyl chains, as found in the ordered lipid lamellar of the SC. In this study the bands at 852, 883, 898 and 935 cm^{-1} were found in the epidermal layers, more specifically the SC. These bands are assigned to CH_3 rocking mode and to the C–N stretching mode, thus reporting about the chain-end conformation. These conformations are associated with different chains of ceramide lipids [49,50]. The basal layer, which is the deepest layer of the epidermis, produces keratinocytes that undergo different developmental stages that start differentiation in the epidermis. The differentiation of cells occurs in the SS and SG with dead cornified corneocytes in the SC. This cornification is a highly complex process involving many structural proteins, fatty acids and lipids, and processing

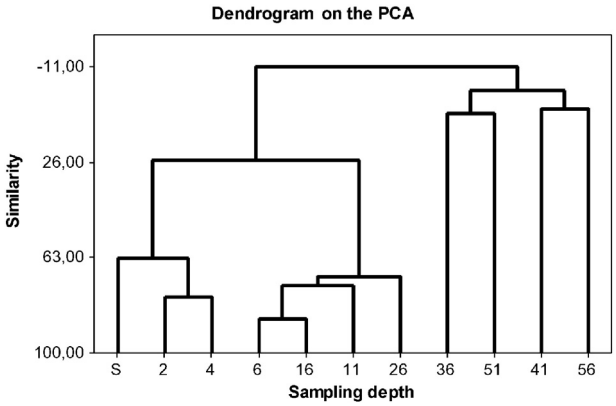

Fig. 1. A dendrogram on the PCA grouping mean spectra in clusters according to their similarity at the 1140–1374 cm^{-1} range. Similarity distance is given in arbitrary units. X axis indicates the skin layer depths in μm.

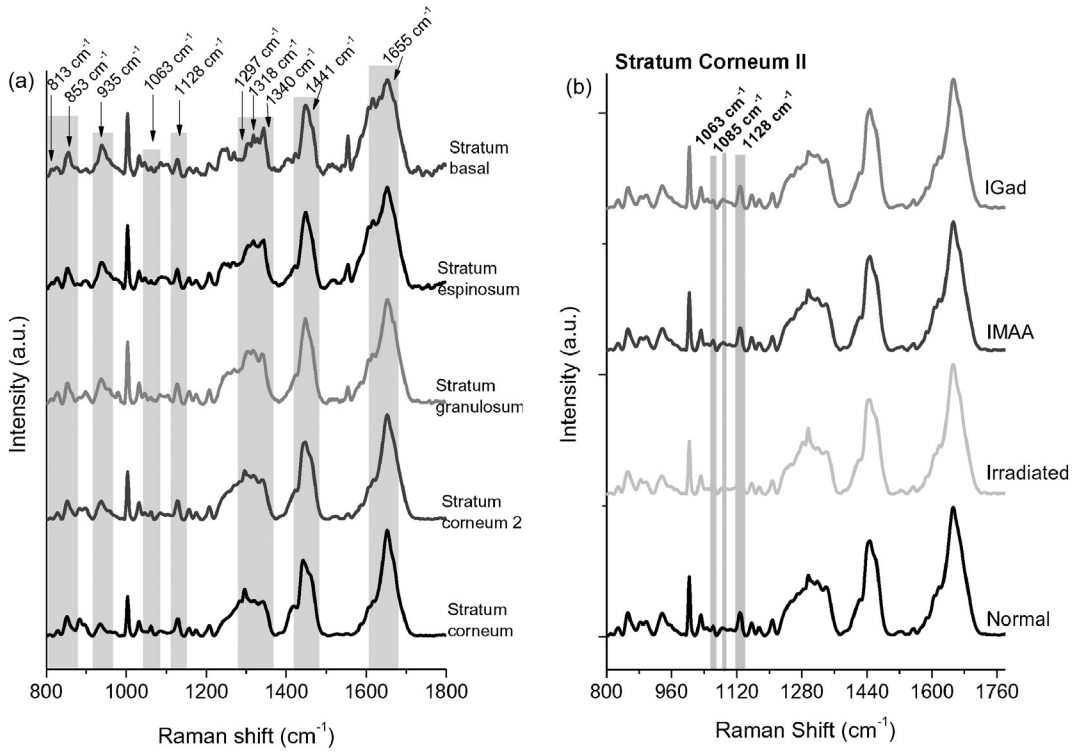

Fig. 2. (a) *In vivo* average spectra of normal skin at different depths (see text). (b) *In vivo* average spectra at the SC2 depth for irradiated MAAs and Gad treated skins, and normal non-irradiated and irradiated skin. The indicated peaks correspond to the characteristic wavenumbers of lipids in the SC.

enzymes. The spectrum corresponding to the basal layer contains specific bands characteristic of DNA and RNA [51]. Although the vibrations assigned to nucleic acids produce low intensity bands, we can identify some of them at 813 (O-P-O), 1318 (DNA, histidine), and 1340 cm^{-1} (DNA) [43,45,52]. No spectral changes, related to vibrational modes of DNA, were identified in the analyzed spectra, which reveal the integrity of the molecule. Each layer contains particular characteristics according to the different treatments. For example, Fig. 2b shows the Raman depth profiles for the region treated with the gel in the SC2. The vibrational peaks shaded correspond to the characteristic wavenumbers of the most representative lipids in the SC2. The vibrational peaks attributed to the gels with MAAs and with Gad were assigned in a previous study [53].

The permeation depth profiles of the gels in the irradiated skin were respectively calculated in terms of the area of the deconvoluted Raman signal assigned to MAAs gels (CH_2 deformation vibrations) with centered peak at 1280 cm^{-1} and Gad gels (CH_2 rocking vibrations) with centered peak at 920 cm^{-1}. The results are shown in Fig. 3. Although their content *versus* depth profiles for both gels reveals a decrease below 2 μm to deeper layers, their behavior differs from each other.

Table 1
Raman shift and assignment of the vibrational bands.

Raman shift (cm^{-1})	Assignment
829	δ (CCH) aliphatic
853	δ (CCH) aromatic, proline
883	δ (CH_2), ν (CC), ν (CN)
935	ρ (CH_3) terminal, ν (CC) α-helix
958	ρ (CH_3), δ (CCH) alkenic
971	ν (CC)
1002	ν (CC) aromatic ring
1031	ν (CC) skeletal *cis*
1063	ν (CC) skeletal *trans*
1085	ν (CC) skeletal random
1128	ν (CC) skeletal *trans*
1157	ν (CC), δ (COH)
1175	ν (CC)
1208	ν (CC_6H_5), Trp, Tyr
1249	δ (CH_2) wagging, ν (CN) amide 3 disordered
1284	ν (CN), δ (NH) amide 3 α-helix
1297	δ (CH_2)
1318	Histidine (DNA)
1342	Guanine, δ (CH)
1384	δ (CH_3) symmetric
1419	δ (CH_3)
1441	δ (CH_2) scissoring
1552	δ (NH), ν (CN) amide 2
1585	ν (C–C) alkenic
1652	*Trans*-urocanic acid
1655	ν (C–O) amide 1 α-helix

ν, stretch; δ, deformation; ρ, rocking; Tyr, tyrosine; Trp, tryptophan.

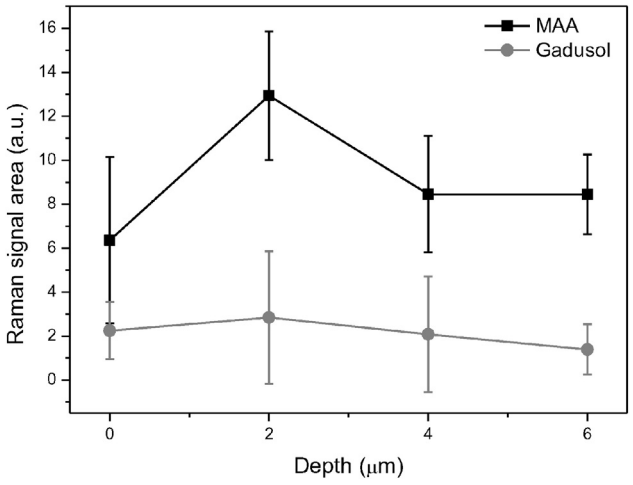

Fig. 3. *In vivo* distribution of MAAs and Gad loaded gels through the stratum corneum calculated from the band area of the Raman signal of MAAs and Gad gels centered at 1280 and 920 cm^{-1}, respectively.

The amount of Gad gel increases by about 26% of the content in the outermost layer of the SC towards 2 μm depth and decreases by about 27% in the 4 μm depth. Whereas, the amount of MAAs gel at 2 μm depth is 103.4% higher than in the outermost layer of the SC and decreases by about 35% at 4 μm. Although the Raman experiments were carried out up to 56 μm depth, the analysis was only done up to 6 μm because at deeper depths the peaks due to the gels vanished.

The *in vivo* confocal Raman spectroscopy method also allowed the evaluation of the *trans*-UCA and histidine variations in the SC of the forearm. Although the levels found of UCA, histidine, and lipids could be related to interindividual variations, the changes of these components in the treated and non-treated skin were found to be significant. The analysis within the range from 1480 to 1720 cm^{-1} and from 1220 to 1370 cm^{-1} in the SC2 of the forearm shows the integrated amounts of *t*-UCA and HIS, respectively, in the SC2 of the forearm (Fig. 4). The average *t*-UCA and HIS amounts were calculated from the Lorentzian curve fitting of UCA (1490–1515 cm^{-1} and 1652 cm^{-1}) [48] and HIS (1318 cm^{-1}) [54] in the Raman spectra regions, before and after UV

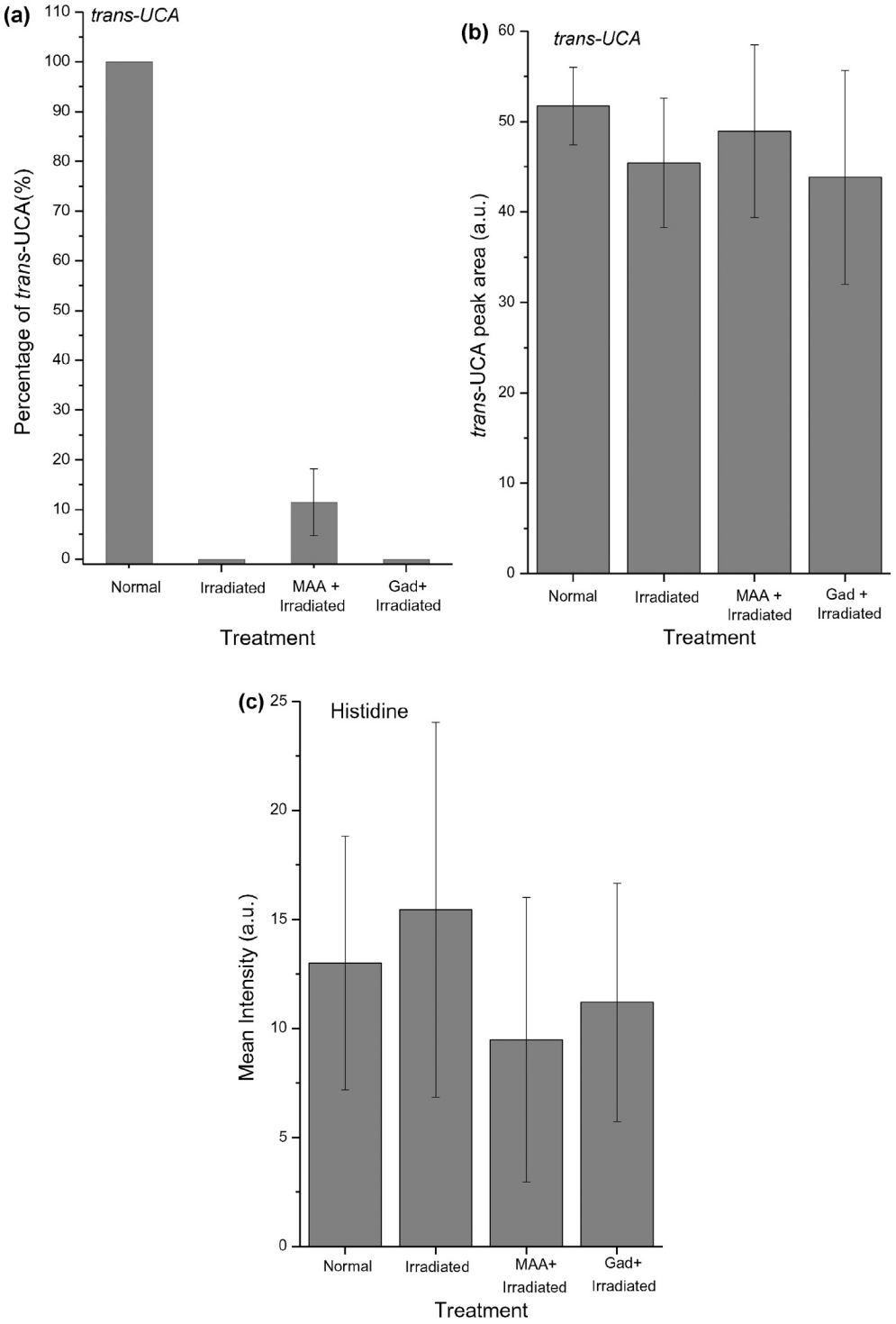

Fig. 4. (a) Percentage difference relative to normal skin in the content of *trans* urocanic acid (1490–1515 cm^{-1}) after treatments; (b) *trans*-urocanic acid (1650 cm^{-1} peak); and (c) histidine integrated areas of Raman bands, respectively. The area values were obtained from Gaussian fitting of the confocal Raman spectrum of the SC before and after treatments.

exposure with or without gels. According to the analysis of the 1652 cm^{-1} peak, the amount of *t*-UCA was higher in the normal skin than in the skin after 3 days of radiation exposure. However, the other peak assigned to the *t*-UCA (1490–1515 cm^{-1}) was not found in irradiated and in irradiated and Gad-treated skin but it was present in irradiated and MAAs-treated skin although in smaller amount than in normal skin. On the other hand, the amounts of HIS in the case of irradiated skin were higher than in normal skin, except for the treated skin with MAAs and Gad, in which they presented a HIS reduction.

The vibrational modes at 1063 and 1128 cm^{-1} correspond to the C–C skeletal stretching vibration of lipids in *trans* conformation, which indicates the predominance of an organized (ordered phase). The vibrational band at 1085 cm^{-1} is simultaneously present in the spectra characterizing the C–C skeletal stretch vibration of lipids in *gauche* conformation in the deeper layer. The areas under these peaks assigned to the lipids were calculated by the Lorentzian deconvolution method (Fig. 5).

Fig. 5 shows an increase of both lipid conformations (*trans* and *gauche*) on irradiated skin compared with normal skin. On the other hand, in the skin with gel applications (Gad and MAAs), the presence of *trans* lipids increases with respect to normal skin but the *gauche* conformation disappears. It is worth mentioning that in some spectra of skin treated with gels, a significant shift of the latter vibrational mode is evident.

4. Discussion

The chronic UV exposure is the main cause of photo-aging and skin cancer. Cole (2001) described the variation of both UVB and UVA measured at 40° N Lat. At this latitude and during a full day in the summer, for perpendicular exposure to the sun's rays without clouds, the incident erythemal dose of the UVA portion of the sun's spectrum radiation is approximately 10 Minimal Erythema Doses (MED), assuming that 1 MED UVA is 10 J/cm^2. The total erythemal dose of UVB under similar situations is approximately 15–20 MEDs, depending on the individual's skin type [5]. Therefore, the energy density used in our study on subjects skin (1.3 J/cm^2) was much lower than the minimum necessary to cause erythema.

The use of sunscreens seems to have become more important in the last decades. Natural products, such as those extracted from algae, have been increasingly used in numerous commercial applications [55]. In this work, SC permeation depth profiles of gels loaded with MAAs and Gad were, for the first time, assessed by *in vivo* Raman spectroscopy (Fig. 2a and b). In the present study, we were able to clearly characterize the differences in human skin epidermis layers, treated and non-treated with irradiation and natural sunscreen loaded polymer gels, according to their similarities in the Raman spectra.

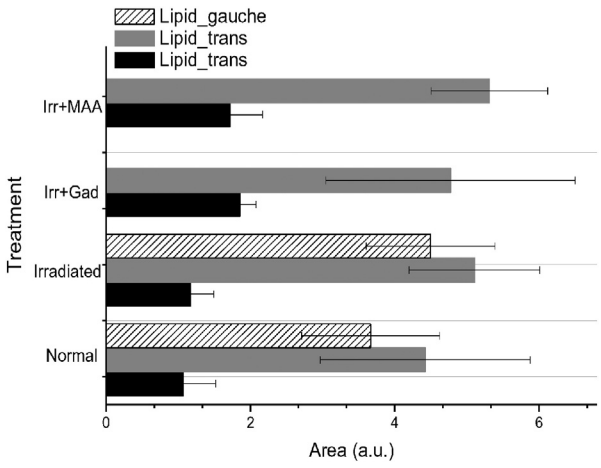

Fig. 5. Area of the peaks assigned to *trans* (black bars: 1063 cm^{-1} and gray bars: 1128 cm^{-1}) and *gauche* (crosshatched bars) conformations of lipids in the SC.

Key information was provided by the Raman intensity of some characteristic peaks related to vibrational modes of polymers and actives, as described in a previous publication [53]. The bands of greater importance in our study correspond to lipids, DNA, and vibrational modes related to UCA and HIS (Fig. 2). The layers of epidermis could be separated using HCA based on their averaged spectra. The mixture between the spectra of the last layers can be explained by their spectral similarity (Fig. 1).

Band areas were correlated with the relative amount of the corresponding compound. This led us to conclude that MAAs and Gad gels were more concentrated at 2 μm depth compared with the surface of the skin (Fig. 3). The gels on the surface reduces the penetration of the actives in the deeper layers of the skin, improving their photostability and decreasing some possible allergenicity [56]. The polymer concentration used (8% w/v) for the preparations formed a gel-like viscous product when refrigerated but had a smooth consistency at room temperature. This hydrogel has an amphiphilic nature characterized by a network of hydrophobic and hydrophilic parts [57]. For this reason, it was expected that the penetration of the gels in the skin would be slightly higher than the values found, because the SC is the principal diffusional barrier of human skin for topically applied substances. A possible explanation comes from a previous finding about Pluronic F127® gels, which is related to the presence of cations of the polymer that attract water molecules. Thus, the surroundings of the chains are less hydrated, which intensifies the OH vibrational modes in the network [53].

Interestingly, even when the concentration of incorporated actives in gels (0.01% w/v) was much lower compared to the concentration of the polymer (8% w/v), changes were observed in some biochemical components of the skin such as UCA and HIS. The photoprotection efficacy of sunscreens is usually calculated on the basis of the prevention of erythema through the use of the SPF (Solar Protection Factor). Other tools, including immune protection efficacy evaluation, could lead to a better method for measuring sunscreen efficacy. In this work, we focused on UCA variations, because it is one of the most important photoreceptors in the SC (Fig. 4a). The peak centered at 1652 cm^{-1} was assigned to *t*-UCA showing a shift in comparison with the literature value (1650 cm^{-1}). The results from the confocal Raman spectroscopy allowed the evaluation of the protective capacity of the sunscreen by monitoring *t*-UCA in the SC after UV exposure. The amount of *t*-UCA decreased after exposure to UV irradiation for 3 days of sessions compared with non-treated skin. These changes were inhibited by the application of gels that maintain the *t*-UCA level close to normal skin. The *t*-UCA photoreceptor isomerizes to *cis*-UCA on the action of UVB radiation specially. The *cis* isomer interacts with a fibroblast cell of skin and stimulates the cells to produce systemic factors. These alter the process of foreign antigens carried by antigen-presenting cell (APC) and the T-cell receptors (TCRs) receive wrong information [58]. Kammeyer et al. suggested that *cis*-UCA increases during UV exposure, and then returns to normal within 10 h. Elimination of *cis*-UCA from the skin may be faster than replacement of *trans*-UCA [59]. According to Egawa et al., the *in vivo* measurement of *t*-UCA amounts is useful for a variety of studies that need continuous measurement of the UCA isomer at the same site, which are not available by conventional invasive methods. They also observed that the decrease in the *trans*-UCA amount was prevented by the application of sunscreen on the skin surface [2,60]. Interestingly, our data show that even using a low concentration of MAA in the gel, the amount of UCA was maintained on average equal to that of normal skin. Considering that UCA isomerization may work as an initiator of the complex pathway leading to immune suppression, the photoprotective properties of MAA look promising for the prevention and therapeutic treatment of skin diseases related to free radicals and UV radiation. The saturation of the natural defense mechanism by high levels of UV radiation exposure could

cause accelerated growth of skin tumor cells. Use of natural actives is an excellent option to protect the skin and avoid allergenic processes.

Trans-UCA is synthesized *in vivo* from the amino acid HIS catalyzed by the enzyme HIS ammonia-lyase in the skin and it is accumulated in the SC because no urocanase activity is present in the epidermis. In this study, we verified that the HIS band area increased in irradiated skin but decreased in skin treated with gels, mainly with the MAAs gel. This behavior is the opposite of which occurred for *t*-UCA. Shibata et al. found that HIS played a very important role to both synthesis of *trans*-UCA and elimination of *cis*-UCA. They suggested that a suitable HIS intake is desirable to protect the skin from UV irradiation to maintain a feedback loop between *cis*- and *trans*-UCA levels [61].

The presence of lipids in the SC is confirmed by the bands located at 1062 and 1128 and 1082 cm^{-1}; the first two modes are assigned to the C–C skeletal stretching vibration of lipids in *trans* conformation and the last one represents the C–C skeletal stretching vibration of lipids in *gauche* conformation [54]. SC is known to be a lipid-rich layer, consisting of cells embedded in the lipid matrix. Two modes related with *trans* conformation of lipids increased their absorbance after irradiation and with the application of both gels. Therefore, this lipid composition change in the SC is evidently related to the lipid chain order. The lipid bilayer of the SC is formed by vesicles from the SG, which flatten and are naturally ordered [62]. The histograms in Fig. 4 show an increase in the *gauche* conformation when the skin was irradiated but this vibrational mode was not found in the skin treated with gels. It may be that the gels lead to an increase in the organization of lipids of SC in comparison to normal skin. The irradiation of the skin generate less water than in normal skin [63]. The order of the superficial lipids and the stimulated skin hydration can lead to reduction of lipid peroxidation [64].

5. Conclusion

This study shows that confocal Raman spectroscopy is a powerful technique to characterize biomaterials like gels in the human skin. This technique allows data to be collected at the molecular level. Our results evidenced gel penetration until 6 μm, *i.e.* within the SC layer. Although the products employed are biocompatible with skin, the polymer can be used to prevent the permeation of damaging substances into deeper skin layers. After 3 days of treatment with UV radiation, the amount of *t*-UCA in the SC decreased and that of HIS increased in comparison with non-treated skin. However, the levels of these compounds remained close to those of normal skin with the applications of gels, thus supporting their protective capacity.

Acknowledgments

We thank the Consejo Nacional de Investigaciones Científicas y Técnicas — CONICET (Argentina). AAM acknowledges CNPq (307809/2013-7) and FINEP (01.10.0661.02-Brazil) for the financial support. Funding from CONICET (PIP0211) and UNMDP (15-E611) are gratefully acknowledged by MSC.

Appendix A. Supplementary Data

Supplementary data to this article can be found online at http://dx.doi.org/10.1016/j.jphotobiol.2015.08.030.

References

[1] A.R. Young, Chromophores in human skin, Phys. Med. Biol. 42 (5) (1997) 789–802.
[2] M. Egawa, H. Iwaki, *In vivo* evaluation of the protective capacity of sunscreen by monitoring urocanic acid isomer in the stratum corneum using Raman spectroscopy, Skin Res. Technol. 14 (4) (Nov. 2008) 410–417.
[3] H. Masaki, Role of antioxidants in the skin: anti-aging effects, J. Dermatol. Sci. 58 (2) (May 2010) 85–90.
[4] A. Anderson, A. Bowman, S.J. Boulton, P. Manning, M. a Birch-Machin, A role for human mitochondrial complex II in the production of reactive oxygen species in human skin, Redox Biol. vol. 2 (2014) 1016–1022.
[5] C. Cole, Sunscreen protection in the ultraviolet A region: how to measure the effectiveness, Photodermatol. Photoimmunol. Photomed. 17 (2001) 2–10.
[6] C.S. Sander, H. Chang, F. Hamm, P. Elsner, J.J. Thiele, Role of oxidative stress and the antioxidant network in cutaneous carcinogenesis, Int. J. Dermatol. 43 (5) (May 2004) 326–335.
[7] F. de la Coba, J. Aguilera, M.V. Gálvez, M. Alvarez, E. Gallego, F.L. Figueroa, E. Herrera, Prevention of the ultraviolet effects on clinical and histopathological changes, as well as the heat shock protein-70 expression in mouse skin by topical application of algal UV-absorbing compounds, J. Dermatol. Sci. 55 (3) (2009) 161–169.
[8] N.K. Gibbs, J. Tye, M. Norval, Recent advances in urocanic acid photochemistry, photobiology and photoimmunology, Photochem. Photobiol. Sci. 7 (6) (2008) 655–667.
[9] F. de fine Olivarius, H.C. Wulf, J. Crosby, M. Norval, The sunscreening effect of urocanic acid, Photodermatol. Photoimmunol. Photomed. vol. 12 (no. 3) (1996) 95–99.
[10] D. Hug, D. Dunkerson, J. Hunter, The degradation of L-histidine and *trans* and *cis*-urocanic acid by bacteria from skin and the role of bacterial *cis*-urocanic acid isomerase, J. Photochem. Photobiol. B vol. 1344 (no. 99) (1999).
[11] E. Menon, H. Morrison, Formation of singlet oxygen by urocanic acid by UVA irradiation and some consequences thereof, Photochem. Photobiol. 75 (6) (2002) 565–569.
[12] N.K. Gibbs, M. Norval, N.J. Traynor, M. Wolf, B.E. Johnson, J. Crosby, Action spectra for the *trans* to *cis* photoisomerisation of urocanic acid *in vitro* and in mouse skin, Photochem. Photobiol. 57 (3) (1993) 584–590.
[13] H.C. Wulf, J. Sandby-Møller, T. Kobayasi, R. Gniadecki, Skin aging and natural photoprotection, Micron 35 (3) (Jan. 2004) 185–191.
[14] P.K. Mukherjee, N. Maity, N.K. Nema, B.K. Sarkar, Bioactive compounds from natural resources against skin aging, Phytomedicine 19 (1) (2011) 64–73.
[15] A. Bhanot, R. Sharma, M.N. Noolvi, Natural sources as potential anti-cancer agents: a review, Int. J. Phytomed. 3 (1) (2011) 09–26.
[16] E.M. Arbeloa, M.J. Uez, S.G. Bertolotti, M.S. Churio, Antioxidant activity of gadusol and occurrence in fish roes from Argentine Sea, Food Chem. 119 (2) (2010) 586–591.
[17] F.R. Conde, M.S. Churio, C.M. Previtali, The deactivation pathways of the excited-states of the mycosporine-like amino acids shinorine and porphyra-334 in aqueous solution, Photochem. Photobiol. Sci. 3 (2004) 960–967.
[18] E.M. Arbeloa, S.G. Bertolotti, M.S. Churio, Photophysics and reductive quenching reactivity of gadusol in solution, Photochem. Photobiol. Sci. 10 (1) (Jan. 2011) 133–142.
[19] J. Ryu, S.-J. Park, I.-H. Kim, Y. Choi, T.-J. Nam, Protective effect of porphyra-334 on UVA-induced photoaging in human skin fibroblasts, Int. J. Mol. Med. (2014) 796–803.
[20] D. Schmid, C. Schürch, F. Zülli, Mycosporine-like amino acids from red algae protect against premature skin-aging, Euro Cosmet. 9 (2006) 1–4.
[21] S.S. Suh, J. Hwang, M. Park, H. Seo, H.-S. Kim, J. Lee, S. Moh, T.-K. Lee, Anti-inflammation activities of mycosporine-like amino acids (MAAs) in response to UV radiation suggest potential anti-skin aging activity, Mar. Drugs 12 (10) (2014) 5174–5187.
[22] A. Sáez, C. Serrano, B. Acha, Model-based classification methods of global patterns in dermoscopic images, IEEE Trans. Med. Imaging 33 (5) (2014) 1137–1147.
[23] S. González, V. Sánchez, a González-Rodríguez, C. Parrado, M. Ullrich, Confocal microscopy patterns in nonmelanoma skin cancer and clinical applications, Actas Dermosifiliogr. vol. 105 (no. 5) (2014) 446–458.
[24] S.E. Godoy, D.a. Ramirez, S.a. Myers, G. von Winckel, S. Krishna, M. Berwick, R.S. Padilla, P. Sen, S. Krishna, Dynamic infrared imaging for skin cancer screening, Infrared Phys. Technol. (2014) 1–6.
[25] T. Subongkot, N. Wonglertnirant, P. Songprakhon, T. Rojanarata, P. Opanasopit, T. Ngawhirunpat, Visualization of ultradeformable liposomes penetration pathways and their skin interaction by confocal laser scanning microscopy, Int. J. Pharm. 441 (1–2) (2013) 151–161.
[26] L. Themstrup, C.a. Banzhaf, M. Mogensen, G.B.E. Jemec, Optical coherence tomography imaging of non-melanoma skin cancer undergoing photodynamic therapy reveals subclinical residual lesions, Photodiagn. Photodyn. Ther. vol. 11 (no. 1) (2014) 7–12.
[27] K.S.K.C.V. Raman, A new type of secondary radiation, Nature vol. 121 (1928) 501–502.
[28] L. Raniero, R.a. Canevari, L.N.Z. Ramalho, F.S. Ramalho, E. a P. dos Santos, R.a. Bitar, K.J. Jalkanen, H.S. Martinho, a.a. Martin, In and *ex vivo* breast disease study by Raman spectroscopy, Theor. Chem. Accounts vol. 130 (no. 4–6) (2011) 1239–1247.
[29] M.G. Tosato, R.S. Alves, E. a P. Dos Santos, L. Raniero, P.F.C. Menezes, K.M.S. Belletti, C.E.O. Praes, A. a Martin, Raman spectroscopic investigation of the effects of cosmetic formulations on the constituents and properties of human skin, Photomed. Laser Surg. vol. 30 (no. 2) (Mar. 2012) 85–91.
[30] P. Oliveira, M. Tosato, R. Alves, Skin biochemical composition analysis by Raman spectroscopy, Rev. Bras. Eng. Biomed. 28 (2012) 278–287.
[31] A. Tfayli, O. Piot, M. Manfait, Confocal Raman microspectroscopy on excised human skin: uncertainties in depth profiling and mathematical correction applied to dermatological drug permeation, J. Biophotonics 1 (2) (May 2008) 140–153.
[32] R. Vyumvuhore, A. Tfayli, H. Duplan, A. Delalleau, M. Manfait, A. Baillet-Guffroy, Raman spectroscopy: a tool for biomechanical characterization of Stratum Corneum, J. Raman Spectrosc. 44 (8) (2013) 1077–1083.
[33] S.M. Ali, F. Bonnier, H. Lambkin, K. Flynn, V. McDonagh, C. Healy, T.C. Lee, F.M. Lyng, H.J. Byrne, A comparison of Raman, FTIR and ATR-FTIR micro spectroscopy for imaging human skin tissue sections, Anal. Methods 5 (9) (2013) 2281–2291.

[34] A.V. Kabanov, E.V. Batrakova, V. Yu, Pluronic block copolymers as novel polymer therapeutics for drug and gene delivery, J. Control. Release 82 (2002) 189–212.
[35] E.V. Batrakova, A.V. Kabanov, Pluronic block copolymers: evolution of drug delivery concept from inert nanocarriers to biological response modifiers, J. Control. Release 130 (2) (Sep. 2008) 98–106.
[36] L. Yildirimer, N.T.K. Thanh, M. Loizidou, A.M. Seifalian, Toxicology and clinical potential of nanoparticles, Nano Today 6 (6) (Dec. 2011) 585–607.
[37] T.S. Moreira, V.P. Sousa, M.B.R. Pierre, Influence of oleic acid on the rheology and *in vitro* release of lumiracoxib from poloxamer gels, J. Pharm. Pharm. Sci. 13 (2) (2010) 286–302.
[38] F.R. Conde, M.S. Churio, C.M. Previtali, The photoprotector mechanism of mycosporine-like amino acids. Excited-state properties and photostability of porphyra-334 in aqueous solution, J. Photochem. Photobiol. B Biol. 56 (2–3) (Jul. 2000) 139–144.
[39] P.A. Plack, N.W. Fraser, P.T. Grant, C. Middleton, A.I. Mitchell, R.H. Thomsont, Gadusol, an enolic derivative of cyclohexane-1,3-dione present in the roes of cod and other marine fish, Biochem. J. 199 (1981) 741–747.
[40] I.R. Schmolka, A review of block polymer surfactants, J. Am. Oil Chem. Soc. 54 (3) (1977) 110–116.
[41] C. Oresajo, T. Stephens, P.D. Hino, R.M. Law, M. Yatskayer, P. Foltis, S. Pillai, S.R. Pinnell, Protective effects of a topical antioxidant mixture containing vitamin C, ferulic acid, and phloretin against ultraviolet-induced photodamage in human skin, J. Cosmet. Dermatol. 7 (4) (Dec. 2008) 290–297.
[42] L. Chrit, C. Hadjur, S. Morel, G. Sockalingum, G. Lebourdon, F. Leroy, M. Manfait, *In vivo* chemical investigation of human skin using a confocal Raman fiber optic microprobe, J. Biomed. Opt. vol. 10 (no. 4) (2005) 44007.
[43] A. Tfayli, O. Piot, F. Draux, F. Pitre, M. Manfait, Molecular characterization of reconstructed skin model by Raman microspectroscopy: comparison with excised human skin, Biopolymers 87 (4) (2007) 261–274.
[44] M. Leroy, J.-F. Labbé, M. Ouellet, J. Jean, T. Lefèvre, G. Laroche, M. Auger, R. Pouliot, A comparative study between human skin substitutes and normal human skin using Raman microspectroscopy, Acta Biomater. 10 (6) (Jun. 2014) 2703–2711.
[45] S. Tfaili, C. Gobinet, G. Josse, J.-F. Angiboust, M. Manfait, O. Piot, Confocal Raman microspectroscopy for skin characterization: a comparative study between human skin and pig skin, Analyst 137 (16) (Aug. 2012) 3673–3682.
[46] A.N.C. Anigbogu, A.C. Williams, B.W. Barry, H.G.M. Edwards, Fourier transform Raman spectroscopy of interactions between the penetration enhancer dimethyl sulfoxide and human stratum corneum, Int. J. Pharm. 125 (1995) 265–282.
[47] T. Greve, K. Andersen, O. Nielsen, ATR-FTIR, FT-NIR and near-FT-Raman spectroscopic studies of molecular composition in human skin *in vivo* and pig ear skin *in vitro*, Spectroscopy 22 (2008) 437–457.
[48] P.J. Caspers, G.W. Lucassen, R. Wolthuis, H. a Bruining, G.J. Puppels, *In vitro* and *in vivo* Raman spectroscopy of human skin, Biospectroscopy vol. 4 (no. 5 Suppl.) (Jan. 1998) S31–S39.
[49] A. Tfayli, E. Guillard, M. Manfait, A. Baillet-Guffroy, Thermal dependence of Raman descriptors of ceramides. Part I: effect of double bonds in hydrocarbon chains, Anal. Bioanal. Chem. 397 (3) (2010) 1281–1296.
[50] E. Guillard, A. Tfayli, M. Manfait, A. Baillet-Guffroy, Thermal dependence of Raman descriptors of ceramides. Part II: effect of chains lengths and head group structures, Anal. Bioanal. Chem. 399 (3) (2011) 1201–1213.
[51] K.H. Hänel, C. Cornelissen, B. Lüscher, J.M. Baron, Cytokines and the skin barrier, Int. J. Mol. Sci. 14 (4) (Jan. 2013) 6720–6745.
[52] Z. Movasaghi, S. Rehman, D.I. ur Rehman, Fourier transform infrared (FTIR) spectroscopy of biological tissues, Appl. Spectrosc. Rev. vol. 43 (no. 2) (Feb. 2008) 134–179.
[53] M.G. Tosato, D.E. Orallo, M.S. Churio, A.A. Martin, C.A.T. Soto, L.E. Dicelio, Influence of mycosporine-like amino acids and gadusol on the rheology and Raman spectroscopy of polymer gels, Biorheology 51 (4–5) (Jan. 2014) 315–328.
[54] Z. Movasaghi, S. Rehman, I.U. Rehman, Raman spectroscopy of biological tissues, Appl. Spectrosc. Rev. 42 (5) (Sep. 2007) 493–541.
[55] D. Schmid, C. Schürch, F. Zülli, H. Nissen, H. Prieur, Mycosporine-like amino acids: natural UV-screening compounds from red algae to protect the skin against photoaging, SÖFW-J. 129 (11) (2003) 38–41.
[56] Y. Gilaberte, S. González, Novedades en fotoprotección, Actas Dermosifiliogr. 101 (8) (Oct. 2010) 659–672.
[57] K.E. Uhrich, S.M. Cannizzaro, R.S. Langer, K.M. Shakesheff, Polymeric systems for controlled drug release, Chem. Rev. 99 (11) (Nov. 1999) 3181–3198.
[58] F.P. Noonan, E.C. De Fabo, Immunosuppression by ultraviolet B radiation: initiation by urocanic acid, Immunol. Today 13 (7) (1992) 250–254.
[59] A. Kammeyer, S. Pavelt, S.S. Asghar, J.D. Bos, M.B.M. Teunissen, Prolonged increase of *cis*-urocanic acid levels in human skin and urine after single total-body ultraviolet exposures, Photochem. Photobiol. 65 (3) (1997) 593–598.
[60] M. Egawa, J. Nomura, H. Iwaki, The evaluation of the amount of *cis*- and *trans*-urocanic acid in the stratum corneum by Raman spectroscopy, Photochem. Photobiol. Sci. 9 (5) (May 2010) 730–733.
[61] K. Shibata, T. Fukuwatari, Effect of dietary histidine content on the change in content of skin urocanic acid isomers in hairless mice irradiated with ultraviolet B, Biosci. Biotechnol. Biochem. 65 (6) (2001) 1415–1418.
[62] D.T. Downing, Lipid and protein struct of mammalian epidermis.pdf, J. Lipid Res. 33 (1992) 301–313.
[63] P.E.R. Thune, The effects of detergents on hydration and skin surface lipids, Clin. Dermatol. 14 (1996) 29–33.
[64] R.L. Roberts, J. Green, B. Lewis, Lutein and zeaxanthin in eye and skin health, Clin. Dermatol. 27 (2) (2009) 195–201.